An integrated model for the evolution of channel morphology, including cohesive bank erosion

A.N. Menéndez[†*], C.E. Laciana[*], P.E. García[†*], J. Rodríguez Ardila[*] & A. Sfriso[*]
[†]*Hydraulics Laboratory, INA (National Institute for Water), Argentina*
[*]*Mathematical Modelling Laboratory, School of Engineering, University of Buenos Aires, Argentina*

ABSTRACT: An integrated hydrodynamic-sedimentologic-morphological model is proposed to deal with the morphological evolution of channel cross-sections in practical situations. While based on a physically sound formulation, efficiency is attained by considering only the relevant physical mechanisms, in view of the geometric scales of the water course, and the time scale of the observer. Its performance is assessed through specific validation tests for the different mechanisms. A numerical experiment is undertaken.

1 INTRODUCTION

Water courses that develop on alluvial material show a changing morphology, determined by the variable water current action. Variations are observed in both the channel depth (bottom evolution) and width (bank evolution). Water acts on the channel boundaries by exerting a shear stress, which depends on the flow velocity. In curved channels, in addition to the longitudinal velocity component, a transversal component also exists, constituting the so called secondary currents.

To numerically simulate these processes, it is necessary to formulate an integrated hydrodynamic-sedimentologic-morphological model. This formulation is conditioned by the geometric scales of the water course, and the time scale of the observer. In this paper, such a model is presented, valid for practical values of those scales.

2 MODEL FORMULATION

2.1 *Hydrodynamic model*

For an open-channel flow problem, we can distinguish locally three 'natural' spatial coordinates: one along the flow direction (longitudinal), a second one in the horizontal plane and across the flow direction (lateral), and a third one in the vertical direction (assuming a mild channel slope). We will consider that, as usual, the characteristic scales are very different in those three spatial directions, allowing for some simplifications. In the first place, it will be assumed that the longitudinal scale of interest (the scale of the observer) is much larger than the transversal dimensions of the cross section, i.e.,

$$L_{ox} \gg \hat{B}, \hat{h} \tag{1}$$

where $\hat{B}$ is a scale for the channel width, $\hat{h}$ a scale for the water depth, and L_{ox} is the longitudinal spatial scale of the observer, which is calculated as (Menéndez 2003) $L_{ox} \equiv \hat{U}\hat{T}$, with $\hat{U}$ being a scale for the longitudinal flow velocity, and $\hat{T}$ the observer time scale. Condition (1) means that the problem can be treated with the 1D approximation (Menéndez 2003), i.e., that the longitudinal variation of the cross-sectional mean flow velocity can be calculated independently of the transversal variation of the flow velocity, using a 1D Longitudinal Model as the well known Saint Venant Equations (Jain 2001).

In the second place, the cross section will be considered as shallow:

$$\hat{B} \gg \hat{h} \tag{2}$$

As a consequence of condition (2), the lateral distribution of flow velocity, if needed, can be determined independently of the vertical distribution.

In the third place, it will be assumed that the lateral spatial scale of the observer L_{oy}, which is calculated as (Menéndez 2003) $L_{oy} \equiv \left(\widehat{\varepsilon_y}\hat{T}\right)^{1/2}$, with $\widehat{\varepsilon_y}$ being a scale for the lateral diffusivity, is at most of the same order of the lateral dimension of the cross section, i.e.,

$$L_{oy} \tilde{<} \hat{B} \tag{3}$$

As a consequence of (3), it is pertinent to calculate the lateral distribution of the longitudinal flow velocity (Menéndez 2003), which may be obtained from a 1D Lateral Model, such as the Lateral Distribution Method (LDM) proposed by Wark et al. (1990):

$$ghI_x - \frac{B_g f}{8}U^2 + h\frac{\partial}{\partial y}\left[\varepsilon_y \frac{\partial U}{\partial y}\right] = 0 \qquad (4)$$

where y is the lateral coordinates measured from the right bankline, $h(y)$ the local flow depth, $U(y)$ the vertically averaged local longitudinal flow velocity, I_x the longitudinal flow slope (obtained from the 1D Longitudinal Model), and f the Darcy-Weisbach friction factor; B_g is a geometrical factor and ε_y the lateral eddy viscosity; they are given by

$$B_g = \sqrt{1+\tan^2\alpha+\tan^2\omega}\,, \quad \varepsilon_y = \chi U_* h \qquad (5)$$

where α is the angle of the longitudinal channel slope, ω the angle of the lateral channel slope (Figure 1), χ the dimensionless lateral eddy viscosity coefficient, and $U_* = \sqrt{\tau_b}$ the shear velocity, with τ_b being the kinematic bottom shear stress, which is parameterized as

$$\tau_b = \frac{1}{8} f B_g U^2 \qquad (6)$$

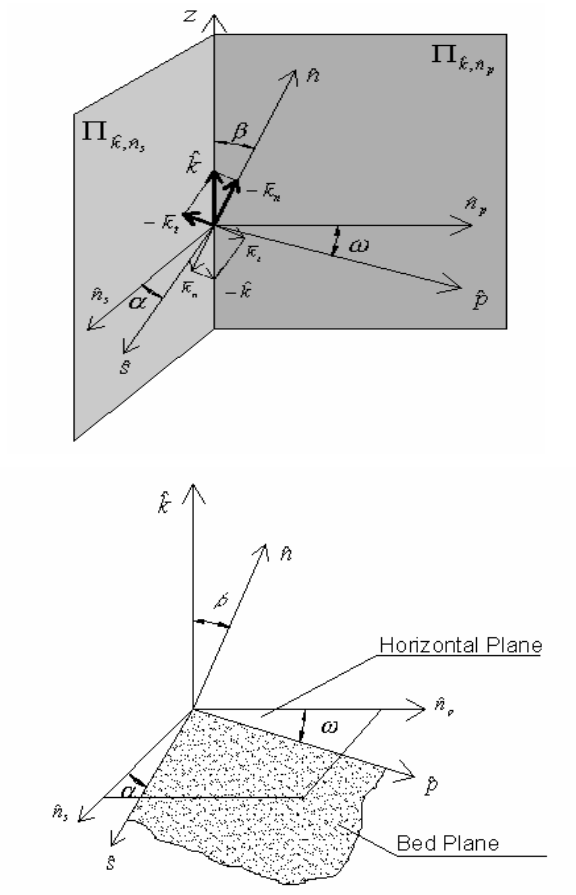

Figure 1. Geometrical parameters.

As boundary conditions for eq. (4), the free-slip condition may be imposed:

$$\left.\frac{dU}{dy}\right|_{\text{bankline}} = 0 \qquad (7)$$

which physically means that the wall boundary layers by the banklines are not solved.

For the present applications, the non linear ordinary differential equation (4) is solved numerically. It is discretized using a centered finite difference scheme. The resultant non linear algebraic system is solved by means of the Newton-Raphson method.

As a consequence of curvature, in addition to the longitudinal flow velocity there are transversal components, which constitute the secondary flow. In particular, the lateral velocity component at the bottom, $u_r(y)$, is of relevance for bed load transport. It has been determined from the parametric vertical velocity profile model of Kikkawa et al. (1976), which assumes that the radius of curvature of the channel is much larger than its width. The expression is the following:

$$u_r = \frac{U^2}{\bar{U}}\frac{h}{r}\frac{1}{\kappa}\left(4.167 - 2.640\frac{1}{\kappa}\frac{\bar{U}_*}{\bar{U}}\right) \qquad (8)$$

where $\bar{U}$ and $\bar{U}_*$ are the transversally-averaged longitudinal flow velocity and shear velocity, respectively, $r = r(y)$ the radious of curvature, and κ von Karman constant (≈ 0.4).

At the banklines it must hold the impenetrability condition

$$u_{rb}\big|_{\text{bankline}} = 0 \qquad (9)$$

The transition between the parametric model value, given by eq. (8), and the bankline value, eq. (9), is taken into account by means of a modulating function, or mask, $M(y)$, with the following form:

$$M(y) = \begin{cases} 1-\left(\dfrac{\delta - y}{y}\right)^{1/2} & \text{if } 0 \le y \le \delta \\ 1 & \text{if } \delta \le y \le B-\delta \\ 1-\left(\dfrac{\delta + y - B}{\delta}\right)^{1/2} & \text{if } B-\delta \le y \le B \end{cases} \qquad (10)$$

where B is the channel top width, and δ the bank boundary layer thickness, which is proposed to scale with the near-bank depth h_b, i.e.

$$\frac{\delta}{h_b} = \kappa_b = const. \qquad (11)$$

where the value of κ_b is to be determined from experimentation. Hence, the lateral bottom flow velocity component is given by

$$u_{rb}(y) = M(y)\,u_r(y)\big|_{\text{model}} \qquad (12)$$

2.2 *Sediment transport model*

Kovacs & Parker (1994) model, based on force balances, is used. In the first place, the forces acting on a sediment particle are considered: the drag force

due to the moving fluid, which is the driving mechanism; the component of the immersed weight of the particle tangential to the plane of the bed, that also constitutes a driving force; and the dynamic Coulomb resistive force, which represents the momentum loss due to collisions. The following equation follows:

$$\left|\vec{u}_\Delta^*\right|\vec{u}_\Delta^* = a\,\tau_{C0}^*\left(\left|\vec{k}_n\right|\hat{t}_{v_p} - \frac{\vec{k}_t}{\mu_C}\right) \tag{13}$$

where $\vec{u}_\Delta = \vec{u}_b - \vec{v}_p$,with $\vec{u}_b$ and $\vec{v}_p$ being the bottom fluid velocity and the particle velocity, respectively, $a \equiv \left(\vec{u}_b / U_*\right)^2$, τ_{C0}^* is the dimensionless shear stress (or Shields parameter) for initiation of motion on a flat bottom, $\hat{t}_{v_p} \equiv \vec{v}_p / \left|\vec{v}_p\right|$ the versor in the direction of the particle velocity, μ_C the dynamic Coulomb friction factor, and $\vec{k}_n$ and $\vec{k}_t$ the components of the vertical versor, pointing downwards, along the normal and transversal directions to the bottom, respectively. The fluid velocity can be expressed as

$$\vec{u}_b = \varepsilon U\ \hat{s}\ +\ u_r\sqrt{1+\cos^2\alpha\tan^2\omega}\ \hat{p}' \tag{14}$$

where $\hat{s}$ is the versor in the longitudinal direction of motion, $\hat{p}'$ the versor on the plane tangent to the bottom and normal to $\hat{s}$, and ε the relation between the longitudinal component of the bottom velocity and the mean transversal velocity *U*.

To solve eq. (13) for the sediment particle velocity, it is proposed to split it into components, by multiplying it alternatively by versors $\hat{s}$ and $\hat{p}'$, obtaining

$$\left|\vec{u}_\Delta^*\right|\left(u_{bs}^* - v_p^*\cos\psi\right) - a\tau_{C0}^*\left(\left|\cos\beta\right|\cos\psi - \frac{\sin\alpha}{\mu_C}\right) = 0 \tag{15}$$

$$\left|\vec{u}_\Delta^*\right|\left(u_{bp}^* - v_p^*\sin\psi\right) - a\tau_{C0}^*\left(\left|\cos\beta\right|\sin\psi - \frac{1}{\mu_C}\frac{\sin\omega\cos^2\alpha}{\sqrt{\sin^2\omega\cos^2\alpha+\cos^2\omega}}\right) = 0$$

where

$$\left|\vec{u}_\Delta^*\right| = \left(u_{bs}^{*2} + u_{bp}^{*2} + v_p^{*2} - 2u_b^*v_p^*\cos\psi - 2u_{bp}^*v_p^*\sin\psi\right)^{1/2} \tag{16}$$

, $v_p = \left|\vec{v}_p\right|$, ψ is the angle between the velocity vector and the *s* direction, and the asterisc indicates dimensionless velocities, with the scale $\sigma \equiv \sqrt{Rgd}$, being *R* the relative grain density, which diameter is *d*. System (15) is solved by means of Newton-Raphson method, to obtain the unknowns v_p^* and ψ .

The dimensionless vectorial volume bedload sediment transport rate per unit normal width (made dimensionless with the scale $d\sigma$) is calculated as

$$\vec{q}_b^* = \xi^*\vec{v}_p^* \tag{17}$$

where ξ^* is the dimensionless volume of particles participating in bedload transport. To obtain this volume, Kovacs & Parker (1994) perform a momentum balance for the bed layer. The generalization of their formulation to include curvature effects leads to

$$\xi^* = \frac{\tau_b^* - \tau_C^*}{\left(\mu_C\left|\vec{k}_n\right|\hat{t}_{v_p} - \vec{k}_t\right).\hat{s}'} \tag{18}$$

where $\hat{s}' = \cos\alpha_s\hat{s} + \sin\alpha_s\hat{p}'$,

$$\tau_b^* = \frac{\varepsilon^2U^2}{aRgd\cos\alpha_s} \tag{19}$$

is the bottom shear stress, and τ_C^* is the dimensionless critical shear stress for initiation of motion. This is obtained by specializing (13) for critical conditions. Taking into account curvature effects, and squaring it, we obtain

$$\left(\frac{\tau_{Cs}^*}{\tau_{C0}^*}\right)^2 + \frac{2}{\mu_C}\frac{\vec{s}_p.\vec{k}_t}{s_p^2}\frac{\tau_{Cs}^*}{\tau_{C0}^*} + \frac{1}{\mu_C^2}\frac{k_t^2}{s_p^2} - \cos^2\beta = 0 \tag{20}$$

where $\vec{s}_p \equiv \sqrt{1+\tan^2\alpha_s}\left(\hat{s} + \tan\alpha_s\hat{p}'\right)$, which physically meaningful solution is

$$\frac{\tau_{Cs}^*}{\tau_{C0}^*} = -\frac{1}{\mu_C}\frac{\vec{s}_p.\vec{k}_t}{s_p^2} + \sqrt{\cos^2\beta + \frac{1}{\mu_C^2}\left[\left(\frac{\vec{s}_p.\vec{k}_t}{s_p^2}\right)^2 - \frac{k_t^2}{s_p^2}\right]} \tag{21}$$

2.3 *Morphologic model*

The channel bottom evolution is calculated through Exner equation, which arises from the sediment mass conservation condition (Raudkivi 1990):

$$\frac{\partial z_0}{\partial t} + \frac{1}{1-\lambda}\left[\frac{1}{r}\frac{\partial}{\partial y}\left(rq_{by}\right) + \frac{\partial q_{bx}}{\partial x}\right] = 0 \tag{22}$$

where z_0 is the bed elevation, *t* the time coordinates, λ the porosity of the bottom sediment, q_{bx} and q_{by} the total stream-wise (longitudinal) and lateral volumetric sediment load per unit width, respectively, and where no suspended sediment load is considered.

For the present applications, uniform longitudinal conditions are assumed, i.e., $\partial/\partial x = 0$. Hence, eq. (22) was discretized by means of a simple explicit centered finite-difference scheme:

$$\frac{\left[z_0\right]_j^{n+1} - \left[z_0\right]_j^n}{\Delta t} + \frac{\left[r\right]_{j+1/2}^n\left(\left[q_{by}\right]_{j+1}^n - \left[q_{by}\right]_j^n\right) - \left[r\right]_{j-1/2}^n\left(\left[q_{by}\right]_j^n - \left[q_{by}\right]_{j-1}^n\right)}{(1-\lambda)\left[r\right]_j^n\Delta y^2} = 0 \tag{23}$$

where *n* is the time coordinate index, and *j* the spatial coordinate index.

Non-cohesive bank erosion is taken into account through the following algorithm, which assumes that the water level is equal to the streambank level (bankfull conditions):

a) After each calculation step, the bank slope at the two border nodes of the calculation domain (in the following, bank-nodes), are determined.

b) If the slope is lower than the critical value, given by the condition $\tan\omega_C = \mu_C$, no action is taken.
c) On the contrary, if the slope is equal or higher than the critical value, a local "slide" process is considered: the bank-node height is lowered so as the slope becomes critical, and a new node (with the streambank level) is added to the calculation domain (towards the exterior of the channel) to represent the new bank location (i.e., it becomes the bank-node for the next time step). To account for mass conservation, the slide volume is next distributed among nodes adjacent to the bank.

If a cohesive stratum exists on top of the non-cohesive bank, the retreat of the latter produces undermining of the former, leading eventually to cantilever type failure. A geotechnical stability analysis is performed which, following Darby and Thorne (1996), includes the effects of positive pore water pressure in the saturated portion, negative pore water pressure in the unsaturated portion, and hydrostatic confining pressure due to the water level in the river, considering a relatively general bank profile geometry. A planar failure type is supposed, common for streambanks destabilized by severe bed degradation (Darby et al. 2000), with the failure plane passing through the top point of the non-cohesive portion of the bank. All possibilities, regarding the relative elevations of water surface, phreatic surface, and tension crack depth are considered, as pointed out by Darby & Thorne (1996), but properly adapted to deal with this specific failure type, as schematized in Figure 2. A search is performed, sweeping the possible fail angle range. Once the safety factor falls below one, the angle corresponding to the minimum cohesion is selected as the fail angle.
The computational treatment of the cohesive stratum is very simple: two nodes (per bank) are used to define it, as shown in Figure 3 as open circles (a third node will be used in the future to indicate the tension crack depth). When a failure is assumed, the bottom node is moved to coincide with the extreme node of the non-cohesive base (black circle), while the top node is located so as to define the failure angle.
The coarse fraction of the failure material is considered to fall at the bank toe, and distribute laterally according to its angle of repose (Figure 4), as proposed by Darby et al. (2002), while the fine fraction is supposed to incorporate to the wash load, and hence ignored. An ad-hoc algorithm was devised to perform the coarse failure material distribution. This material is then treated as non-cohesive material of a mean grain diameter different from that associated to the bottom sediment.

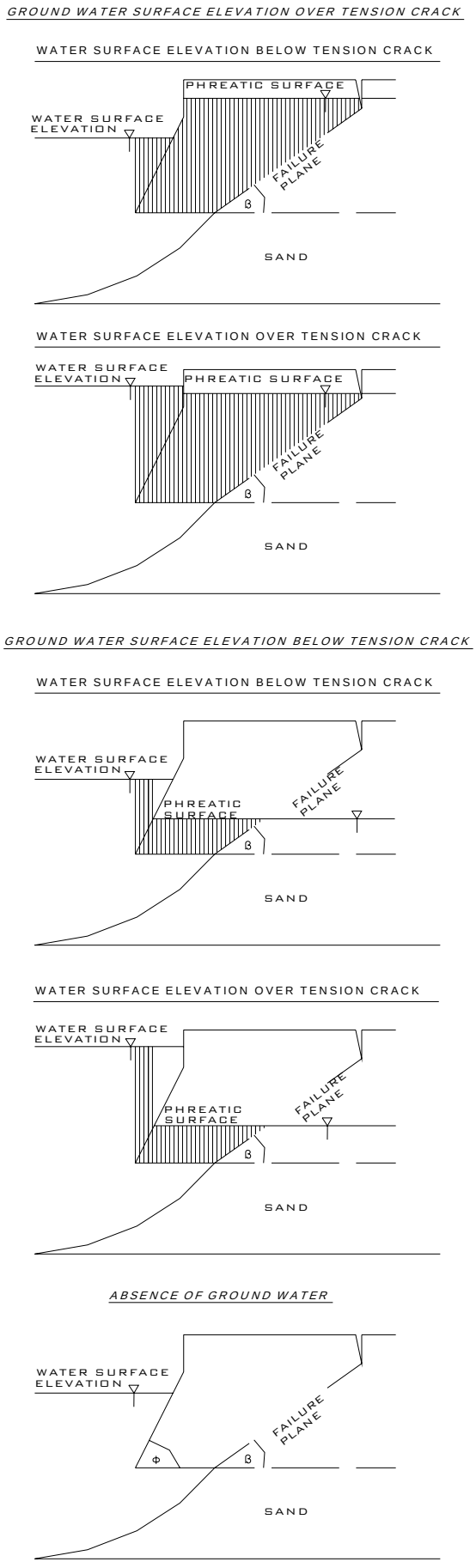

Figure 2. Bank failure cases.

3 VALIDATION

3.1 *Validation strategy*

In order to validate the proposed integrated model, the effects of the main erosion mechanisms are tested separately, comparing the model predictions with existing experimental data and/or previous calculation results. In the first place, a straight channel with non-cohesive banks is considered, so as to check that the methodology can successfully deal with the original problem of Kovaks and Parker (1994). In the second place, a curved, fixed banks channel is taken, where the incorporated secondary flow effects are validated. For both cases, uniform longitudinal conditions are assumed, i.e., $\partial / \partial x = 0$. The time evolution of the channel cross section is analyzed. In the third place, the cohesive stratum failure algorithm is tested. The validation of the procedure for the treatment of the failure material is still under way.

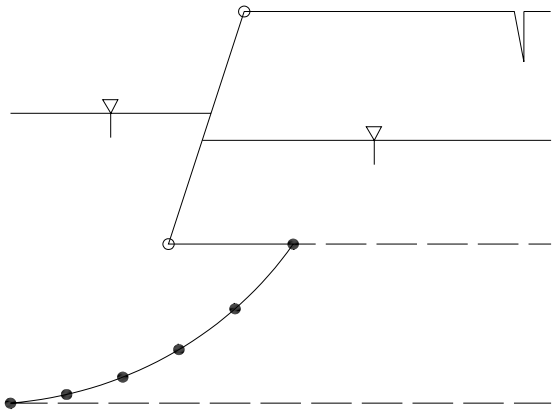

Figure 3. Cohesive-bank nodes (open circles).

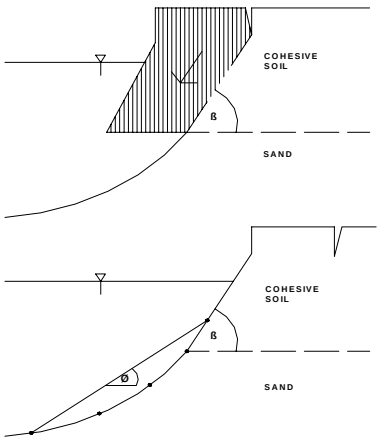

Figure 4. Distribution of failure material

3.2 *Straight channel with non-cohesive banks*

The experiments performed by Ikeda (Kovacs & Parker 1994) are chosen as the first validation test. The channel is straight, prismatic, and symmetric, with a 0.220 m base width, and a longitudinal slope of 0.00215. The initial channel cross section is trapezoidal, with bottom and banks made of sand, with mean diameter d_{50} = 1.3 mm. The initial depth was 0.061 m The model parameters were fixed at the values used by Kovacs & Parker (1994). The initial lateral model domain was discretized into 100 intervals, resulting a spatial step $\Delta y = 0.00438$ m. The temporal step was chosen as $\Delta t = 1$ second, which produces a bed elevation change no larger than 1 mm per time step, thus providing enough accuracy to the solution, while preserving numerical stability.
Figure 5 presents the comparison for the (right half-) channel cross section evolution between the present numerical results and the ones obtained by Kovacs & Parker (1994), identified as K&P in the figure. The latter authors used a 2D transversal hydrodynamic model, i.e., they did not decouple the vertical and lateral directions of motion, and took into account the vertical velocity component, which lead to a more complex calculation procedure. Additionally, they pushed the validity of their bed load transport model beyond the water surface, to account for sediment delivery from the dry bank. The very satisfactory agreement between the two solutions observed in Figure 5 indicates that the present simpler, but physically sound, approach is good enough to capture all the relevant phenomena.

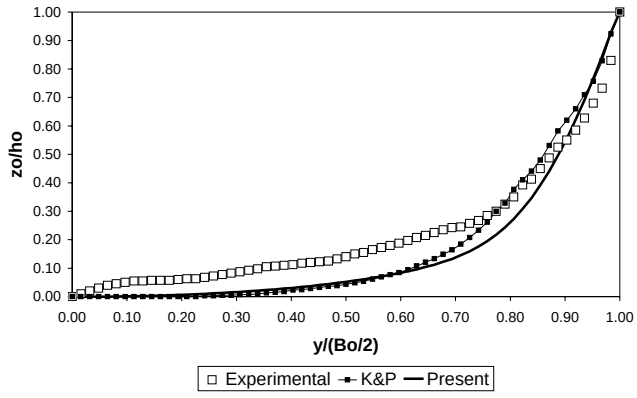

Figure 5. Comparison between K&P and present model results for the cross section evolution.

In Figure 6 the normalized (left half-) channel profile (B_o is the initial bottom width, and h_o the initial centerline depth) according to both models and Ikedas's experimental results, are presented. It is observed that K&P model seems to capture more accurately the bank slope, which could be due to their more elaborated hydrodynamic and bank erosion model. The deviations of the experimental data from the model results in the bottom zone are thought to

be due to the presence of bottom forms, not included in the present theory.

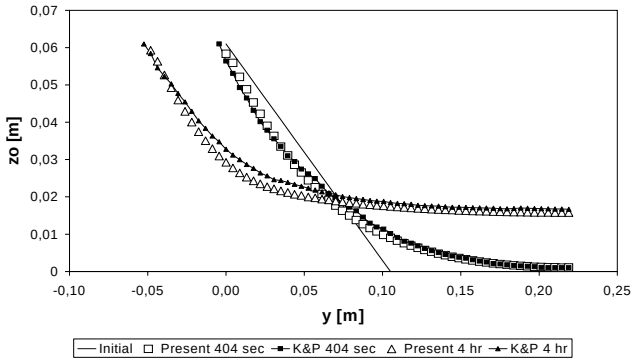

Figure 6. Comparison of K&P and present model results with experimental results for the cross section form after 12 hours.

Similar comparisons are presented in Figure 7 for the time evolution of the top width W and centerline depth h, relative to their initial values (W_o is the initial top width). In the case of the top width, it is observed that the present approach, which gives stair-like responses due to the impulsive nature of the bank erosion algorithm, follows the trend of K&P results, with both of them overestimating the experimental rate of increase at the initial stages, but improving the agreement as time flows. Regarding the centerline depth evolution, the present model provides a better overall agreement with experimental results.

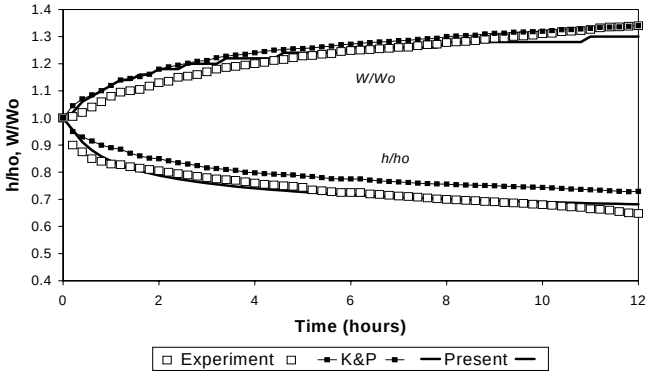

Figure 7. Comparison of K&P and present model results with experimental results for the top width and depth evolution.

3.3 *Curved channel with fixed banks*

The second validation test refers to the experiments performed by Kikkawa et al. (1976). The experimental apparatus was a curved open channel, with vertical rigid walls, bed width B_o = 1 m, longitudinal bottom slope I_x = 0.002, initial uniform depth h_o = 0.063 m, sand bed with d_{50} = 0.9 mm, and curvature radius varying from 4 m at the inner bank to 5 m. at the outer one. The flow discharge was 30 l/s.

The channel width was represented with 100 intervals, which gives a spatial step Δy = 0.01 m. A temporal step Δt = 1 second was taken, which produces a bed elevation change no larger than 1 mm per time step, keeping the numerical solution accurate enough.

Taking as bank- depth h_b the one corresponding to the node adjacent to the bank-node, the best results were obtained for κ_b = 420.

Figure 8 shows the comparison between model predictions and experimental data, using Kikkawa et al. (1976) lateral velocity model, which in the following will be called, for simplicity, Kikkawa model. The agreement is considered as satisfactory, in view that the model represents the correct evolution trend and gives the right magnitude of the bottom height change. The most significant qualitative and quantitative departures occur close to the left bank (y = W_o).

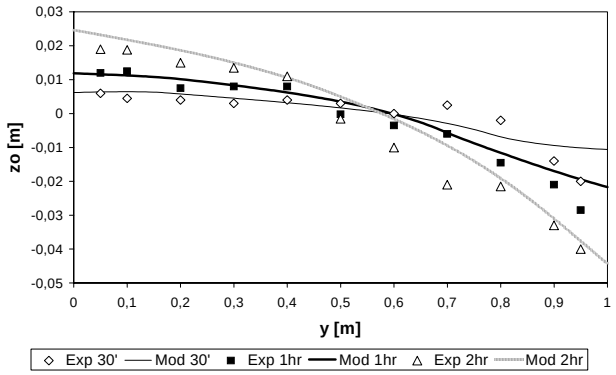

Figure 8. Comparison between experimental data and model results using Kikkawa lateral velocity model.

3.4 *Failure of cohesive stratum*

The third validation test consisted in comparing the failure angle of the cohesive stratum as predicted by the present model and Darby et al. (2000) model (the computer program was kindly made available to the authors by request), for the particular case of the failure plane passing through the toe of the stratum (the only matching situation between the two models). The stratum height was taken as 5.86 m, with an initially practically vertical bank slope (89º), in order to guarantee unstable conditions, and a tension crack depth of 2 m. The soil parameters were selected as follows: cohesion = 14.9 kN/m^2, friction angle = 29º, and specific weight = 20.9 kN/m^3. For two phreatic surface depths (relative to the stream-bank level), different water surface depths were used. Table 1 shows the comparisons between the results obtained from both models. It is observed that the fail angles provided by the two models are very similar, so the present formulation is consid-

ered as validated, taking into account that some truncation errors occur during the angle searching.

Table 1. Fail angle for different phreatic and water surface depths.

Experiment	1	2	3	4	5	6
Phr. Surf. depth (m)	1.27	1.27	1.27	3.27	3.27	3.27
Wat. Surf. Depth (m)	4.27	3.27	2.27	5.27	4.27	3.57
Fail angle Darby(º)	59	59	59	59	59	59
Fail angle Present (º)	57	56	55	58	59	58

4 NUMERICAL EXPERIMENT

A numerical experiment was performed for an initially very unstable straight channel, with a trapezoidal form 22 m wide, 9 m deep, and 20º bank slopes. The non-cohesive base stratum has d_{50} = 0.130 mm and a friction angle of 20º, while the cohesive stratum (at both banks) is 3 m thick, with cohesion 20 kN/m^2. The spatial step is 0.43 m, while the time step amounts to 1 second.

The channel cross-sectional form evolves very fast during a single day, increasing its width about three times, and reducing its depth to about half the initial value. Figure 9 shows the cross-section form for different instants of time. It is observed how the widening process proceeds through undermining and failure of the cohesive strata, while the non-cohesive base flattens, with its bottom level growing. The failure material is not considered. The small asymmetry observed between the two banks is due to round-off errors, which sometimes trigger bank failure with a difference of one computational time step.

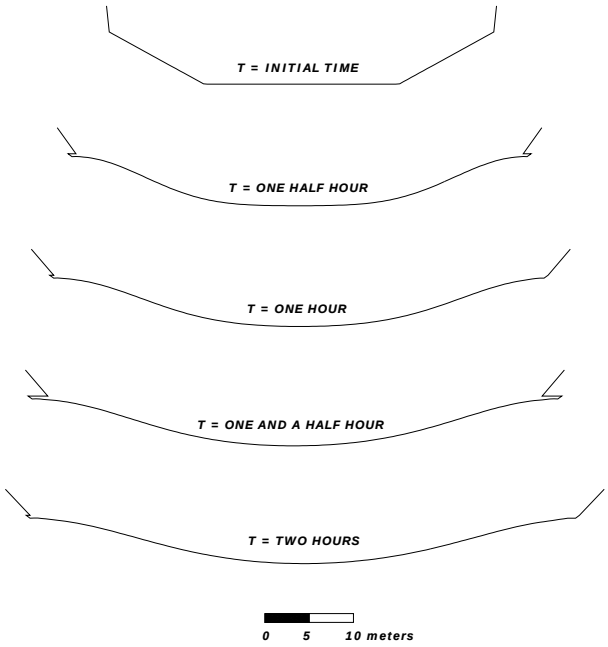

Figure 9. Cross-sectional (undistorted) form for different instants of time.

As an illustration, Figure 10 presents a detail of the

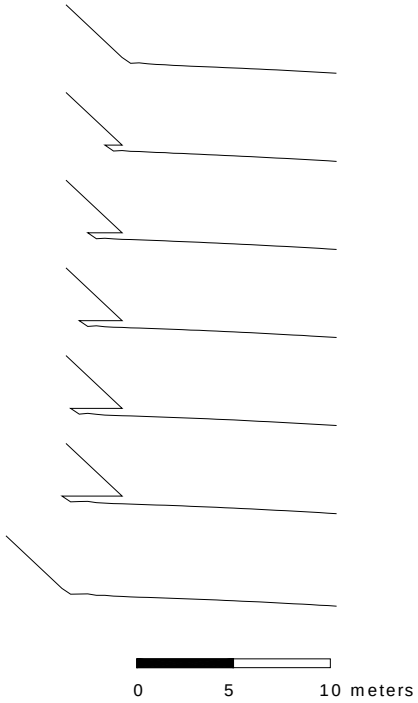

undermining process, till failure, for the right bank.

Figure 10. Undermining process for the right bank. Cross section each half hour, since 16.5 hours after start.

5 CONCLUSIONS

The integrated hydrodynamic-sedimentologic-morphological model proposed in the present paper constitutes an efficient tool to deal with the morphological evolution of channel cross-sections in most practical situations, i.e., while based on a physically sound formulation, it preserves simplicity by considering only the relevant physical mechanisms. The treatment of the non-cohesive bank base and the cohesive bank upper stratum has been validated separately, thus expecting that their combined action performs well. Work is still under way to incorporate the failure material.

6 REFERENCES

Darby, S.E. & Thorne, C.R. 1996. Development and Testing of Riverbank-Stability Analysis, *Jr. of Hydr. Eng.*, **122**, 8, August, 443-454.

Darby, S.E., Gessler, D. & Thorne, C.R. 2000. Computer Program for Stability Analysis of Steep, Cohesive Riverbanks, *Earth Surface Processes and Landforms*, **25**, 175-190.

Darby, S.E., Alabyan, A.M. & Van de Wiel, M.J. 2002. Numerical simulation of bank erosion and channel migration in meandering rivers, *Water Resources Research,* **38**, 9.

Jain, C. 2001. *Open-Channel Flow*. John Wiley and Sons, New York.

Kikkawa, H., Ikeda, S. & Kitagawa, A. 1976. Flow and Bed Topography in Curved Open Channels", *Journal of the Hydraulics Division*, **102**, HY9, September, 1327-1343.

Kovacs, A. & Parker, G. 1994. A new vectorial bedload formulation and its application to the time evolution of straight river channels, *J. Fluid Mech.*, **267**, 153-183.

Raudkivi, A.J. 1990. *Loose Boundary Hydraulics*, 3rd Edition, Pergamon Press, New York.

Menéndez, A.N. 2003. Selection of optima mathematical models for fluvial problems", *Proc. Third IAHR Symposium on River, Coastal and Estuarine Morphodynamics, September*, Barcelona, Spain.

Wark, J.B., Samuels, P.G. & Ervine, D.A. 1990. A practical method of estimating velocity and discharge in a compound channel. In W.R. White (ed.), *River Flood Hydraulics*, John Wiley & Sons, Inc., Chichester, UK, 163-172.